JACS
JOURNAL OF THE AMERICAN CHEMICAL SOCIETY
pubs.acs.org/JACS

Article

Cooperative Gating of a K^+ Channel by Unmodified Biological Anionic Lipids Viewed by Solid-State NMR Spectroscopy

Maryam Yekefallah,[‖] Evan J. van Aalst,[‖] Roy A. M. van Beekveld, Isaac R. Eason, Eefjan Breukink, Markus Weingarth, and Benjamin J. Wylie*

Cite This: J. Am. Chem. Soc. 2024, 146, 4421−4432

Read Online

ACCESS | Metrics & More | Article Recommendations | Supporting Information

ABSTRACT: Lipids adhere to membrane proteins to stimulate or suppress molecular and ionic transport and signal transduction. Yet, the molecular details of lipid−protein interaction and their functional impact are poorly characterized. Here we combine NMR, coarse-grained molecular dynamics (CGMD), and functional assays to reveal classic cooperativity in the binding and subsequent activation of a bacterial inward rectifier potassium (Kir) channel by phosphatidylglycerol (PG), a common component of many membranes. Past studies of lipid activation of Kir channels focused primarily on phosphatidylinositol bisphosphate, a relatively rare signaling lipid that is tightly regulated in space and time. We use solid-state NMR to quantify the binding of unmodified ^{13}C-PG to the K^+ channel KirBac1.1 in liposomes. This specific lipid−protein interaction has a dissociation constant (K_d) of ∼7 mol percentage PG (X_{PG}) with positive cooperativity (n = 3.8) and approaches saturation near 20% X_{PG}. Liposomal flux assays show that K^+ flux also increases with PG in a cooperative manner with an EC_{50} of ∼20% X_{PG}, within the physiological range. Further quantitative fitting of these data reveals that PG acts as a partial (80%) agonist with fivefold K^+ flux amplification. Comparisons of NMR chemical shift perturbation and CGMD simulations at different X_{PG} confirm the direct interaction of PG with key residues, several of which would not be accessible to lipid headgroups in the closed state of the channel. Allosteric regulation by a common lipid is directly relevant to the activation mechanisms of several human ion channels. This study highlights the role of concentration-dependent lipid−protein interactions and tightly controlled protein allostery in the activation and regulation of ion channels.

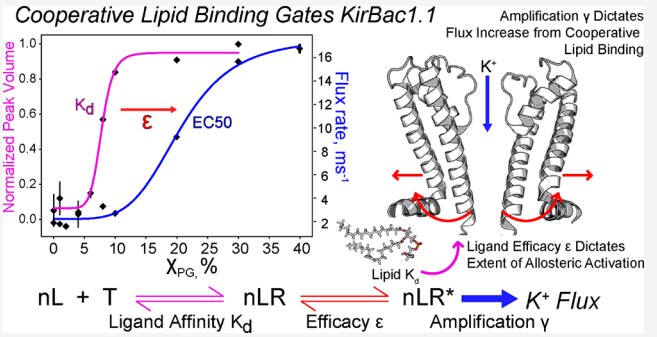

INTRODUCTION

Membrane proteins perform vital tasks that must be tightly regulated, including cellular molecular transport[1] and signal transduction.[2] Many membrane proteins are directly activated, inactivated, or otherwise regulated by specific lipid types, driving dynamic conformational exchange in their native lipid environments.[3] Activating ligands and stimuli, including membrane lipids, can elicit a cooperative allosteric response from their partnered proteins, but these effects are largely unexplored. Unfortunately, it is difficult to specify and quantify this cooperativity, as lipid−protein interactions are challenging to identify and directly relate to protein function. Extant studies use nitroxide or fluorescently labeled lipids, which potentially alter the native lipid−protein molecular recognition. It is crucial that these relationships are better understood as cooperative binding allostery is an important feature in biological systems, including cellular signaling and transport processes.[4] A sigmoidal relationship between ligand binding and overall tissue response is the hallmark of processes that must be carefully regulated within living organisms.[5] The cooperative association of lipids to membrane proteins is likely a fundamental regulation mechanism but under-identified.

K^+ channels are tetrameric proteins, and past work suggested that the subunits may act cooperatively during channel gating.[6−8] This process is in response to gating stimulus, which could be a change in transmembrane voltage or ligand association, including Ca^{2+},[9,10] or phosphatidylinositol bisphosphate (PIP_2).[11,12] Inward-rectifier K^+ (Kir) channels are membrane proteins that prefer inward K^+ conductance into the cell.[13,14] They are endemic to excitable cells, especially in the brain and heart, and a malfunction induces multiple disorders including Parkinson's, heart disease, and kidney dysfunction.[14,15] Both prokaryotic and eukaryotic Kir channels share a common activation motif, where anionic phospholipids like

Received: August 24, 2023
Revised: January 23, 2024
Accepted: January 24, 2024
Published: February 9, 2024

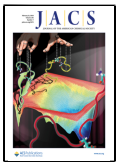

https://doi.org/10.1021/jacs.3c09266
J. Am. Chem. Soc. 2024, 146, 4421−4432

PIP_2 and phosphatidyl glycerol (PG) directly bind to a highly cationic lipid-binding domain at the intracellular water−lipid interface to act as allosteric effectors and induce channel activation and conductance.[16−22] Past work showed that these channels may gate cooperativity, where interaction of one subunit with a gating ligand triggers increased ligand affinity in other subunits. If cooperativity does universally exist in K^+ channel gating and permeation, it would be a crucial means to establish and regulate the membrane potential. Indeed, mutation of the anionic lipid binding pocket in Kir2.1 increased the lifetime of subconductance states, indicating a reduction of the dose response from PIP_2 gating and an increase in basal activity and ultimately suggesting that the gating response was no longer tightly regulated.[12] However, many studies make use of water-soluble PIP_2 analogues as Kir channel activators, which negate any synergistic effects from lipid acyl chains to the transmembrane hydrophobic surface. Recent work has suggested that protein-acyl chain interactions are crucial for K^+ conductance.[23] Studies of G protein-activated (GIRK) channels found that activated $G\beta\gamma$ dimers gated the protein cooperatively.[7,8,24] Although illuminating, these experiments each examined only individual steps in the ligand association, activation, and conductive cycle of the K^+ channels. Likewise, the stoichiometry between the protein and gating ligand was undefined, leaving it completely ambiguous if cooperativity between subunits was analogous or otherwise reflected in association with the gating ligand. Further experiments are required to understand how each step in the gating process is coordinated in concert by a native lipid activator.

In this report, we use uniformly ^{13}C enriched natural PG lipids,[25] which are otherwise unaltered, isolated from bacteria to determine the binding affinity and cooperativity in lipid gating of the bacterial Kir channel KirBac1.1.[26] Like other Kir channels, KirBac1.1 is activated by anionic lipids including PG.[16,27] Bilayer cholesterol will also either activate or deactivate the channel, depending on the concentration.[28−30] Anionic lipids activate KirBac1.1 by triggering a series of concerted motions and structural rearrangement in the transmembrane region along an allosteric network linking PG binding to channel activation.[31] The role of PG in KirBac activation is directly analogous to the PIP_2 activation of hKir. Many of the features of PG activation of KirBac may be closely related to PG and phosphatidic acid (PA) interaction with other human channels such as the mechanosensitive channel TREK-1.[32,33] Furthermore, PA and PG may directly bind to Kir2.1 and Kir2.2 to cooperatively enhance PIP_2 activation of these channels.[34,35] Thus, understanding cooperativity in PG-driven activation of KirBac1.1 will inform on the lipid activation of hKir channels and may also provide insight into how PG specifically might interact with other human ion channels.

Previously, we identified that gating arginine residues were directly responsible for channel activation,[16] and subsequent work showed that tryptophan side chains were also essential for anionic lipid recruitment.[36] Ultimately, however, a fundamental question was left unanswered: what is the affinity of KirBac1.1 for anionic lipids, and what role, if any, do lipid−protein cooperativity and intersubunit cooperativity play in the activation of KirBac1.1? Lipid−protein dissociation constants (K_d's) are rarely known due to complications in experimentally measuring such events in a native or native-like environment, which is unfortunate as these interactions govern and regulate a myriad of biological responses. To address these questions, two-dimensional magic-angle spinning (MAS) SSNMR experiments were performed, revealing chemical shift perturbations (CSPs) in ^{13}C-PG upon the addition of natural abundance KiBac1.1, corresponding to the lipid−protein complex. CSPs of interest in the headgroup region of PG were resolved in 1D direct polarization (DP) experiments with ^{13}C-PG at successively higher mole percentages (X_{PG} = [mol of PG]/[mol of total lipids]) in proteoliposome samples. The results of this titration indicated that the lipid−protein dissociation constant, K_d, is 7% X_{PG} with positive Hill-type cooperativity (n = 3.8). In tandem, we performed coarse grain molecular dynamics (CGMD) simulations with different X_{PG} values and calculated total PG residency time as a function of PG concentration. K_d extracted from PG residency time data was largely consistent with the experimental data. Fluorescence K^+ efflux assays were performed indicating that the rate of K^+ flux as a function of PG concentration is also sigmoidal and cooperative but with an EC_{50} nearly three times the K_d. These results were reconciled using the Signal Amplification (γ), Binding affinity (K_d), and Receptor activation Efficacy (ε) (SABRE) equation.[37,38] This treatment revealed that PG lipids act as potent but incomplete agonists of KirBac1.1 and amplify the rate of K^+ flux as a function of cooperativity in lipid loading onto KirBac1.1. Our results have unique implications in lipid cooperativity throughout the allosteric and regulation cycle of a membrane protein.

MATERIALS AND METHODS

Expression and Purification of KirBac1.1. Expression of Kirbac1.1 was performed as described previously.[31] In summary, the Kirbac1.1 "WT" plasmid containing the stability mutant (I131C) was used, which does not have an effect on the activity and gating of the channel[39] and is referred to as SM-KirBac1.1 throughout the manuscript. The plasmid was also engineered to include a C-terminal hexahistidine (6xHis) tag for purification purposes. The U-^{13}C,^{15}N M9 minimal medium was used for NMR sample growth, and the Terrific Broth medium was used for the natural abundance (NA) cell growth for assay samples. One millimolar isopropyl β-D-1-thiogalactopyranoside (IPTG) was used for the induction of cells at OD_{600} ∼ 0.9−1. Cells were harvested after ∼18 h of expression at 18 °C and kept at −80 °C until the protein was extracted and purified. Frozen cells were resuspended using a lysis buffer (50 mM Tris-base pH 8, 150 mM KCl, 250 mM sucrose, and 10 mM $MgSO_4$) and lysis cocktail (1 mM benzamidine, 1 mM phenylmethylsulfonyl fluoride, 0.2 mg/mL lysozyme, 0.2 mg/mL RNase, protease inhibitor tablets (Thermo)) at 5 mL/g cells. Resuspended cells were homogenized at 10−15 psi, and then 30 mM decyl-β-D-maltopyranoside (DM) was added for extraction of the membrane proteins (between 3 and 4 h at 4 °C with rocking). Ultracentrifugation was used to separate the debris, and detergent-solubilized membrane proteins in the supernatant were filtered to be loaded onto a 5 mL Histrap column (Cytiva). The NMR Exchange Buffer (50 mM Tris-base pH 7.5, 50 mM KCl, 5 mM DDM, 1 mM EDTA) for NMR samples or regular exchange buffer (50 mM Tris-Base pH 8, 150 mM KCl, 5 mM DDM, 1 mM EDTA) for assay samples was used in desalting followed by size exclusion chromatography (SEC) steps. The tetrameric protein fractions were collected from the SEC column, concentrated to ∼1 mg/mL for reconstitution steps, and stored at 4 °C until needed.

Expression and Purification of Isotopically Enriched PG Lipids. PG was isolated, and quality was assessed as described previously.[25] In brief, *Staphylococcus simulans* was grown for 16 h at 37 °C and 220 rpm in Luria broth (LB) followed by resuspension of the appropriate amount of cells in isotopically enriched media to reach OD_{600} = 0.05. Isotopically enriched media were composed of 60 v/v% ^{13}C,^{15}N Silantes OD2 (Cambridge Isotopes), 0.5 v/v% ^{13}C,^{15}N

https://doi.org/10.1021/jacs.3c09266
J. Am. Chem. Soc. 2024, 146, 4421−4432

BioExpress (Cambridge Isotopes), 2 g/L U-^{13}C-D-glucose, 1 g/L U-$^{15}NH_4Cl$, 6 g/L Na_2HPO_4, 3 g/L KH_2PO_4, and 0.5 g/L NaCl. Bacteria (1 L of total culture per 2 L baffled flask) were incubated for 6h to reach a final OD_{600} = 4.5, harvested, and then treated with lysozyme for 2 h. Following the Bligh−Dyer[40] total lipid extraction methodology, bacteria were resuspended in phosphate-buffered saline (PBS), and subsequently 2 vol of MeOH and 1 vol of $CHCl_3$ were added, after which the mixture was vigorously stirred for 1 h at room temperature. Then, 1 vol of $CHCl_3$ followed by 1 vol of PBS was added, and the organic phase was collected and evaporated to dryness. The dried lipids were then resuspended in $CHCl_3$ and loaded onto a silica (silica 60, 0.040−0.063 nm) column that was equilibrated in $CHCl_3$. Finally, PG was obtained by running an isocratic elution of 48:48:3:1 $CHCl_3$/EtOH/H_2O/NH_3, and the obtained fractions were assessed by TLC (in the same solvent) and solution-state NMR.

Reconstitution of NMR and Assay samples. Natural abundance (NA) 1-palmitoyl-2-oleoyl-glycero-3-phosphocholine (POPC) from Avanti Polar Lipids and ^{13}C-labeled PG were used to make lipid films for the lipid-labeled NMR samples, and NA POPC and POPG (3:2, or 40% X_{PG}) from Avanti were used for the transferred echo double resonance (TEDOR) experiment and assay samples. Lipids were mixed at the desired ratio in a glass vial, dried under N_2 gas for 10−15 min, and left under a vacuum overnight to fully remove the chloroform. Dried films were resuspended using a nondetergent NMR buffer (50 mM Tris-base pH 7.5, 50 mM KCl, 1 mM EDTA) for NMR samples and K^+ buffer (20 mM K-HEPES, 150 mM KCl, 1 mM EDTA, pH 7.4) for assay samples to have a final concentration of 5 mg/mL of lipids. Liposomes were formed by 5−15 min of mild sonication (cycles of 2 min on and 2 min off) to prevent sample overheating using a VWR Symphony Ultrasonic Bath. 3-[(3-Cholamidopropyl)dimethylammonio]-1-propanesulfonate (CHAPS, 18.5 mM) was used to destabilize the bilayers. The lipid/detergent mixture was equilibrated on the bench for 2−3 h. Concentrated Kirbac1.1 was added to the mixture in 1:1 w/w ratio (lipid/protein, corresponding to an approximately 50:1 molar ratio) for NMR samples and 200:3 w/w for assay samples. Assay samples for validating the functionality of purified PG were made using the same protocol with 40% X_{PG} and a 200:3 w/w lipid/protein ratio. Lipids and protein were annealed for an hour, and then the NMR samples were diluted with the NMR nondetergent buffer. Biobeads (Bio-Rad) were added to facilitate detergent removal and proteoliposome formation. Biobeads were added twice daily until the samples turned cloudy, and no trace of detergent was observed.

NMR Sample Preparation. Proteoliposomes were centrifuged at 70,000 rpm for 1.5 h and 4 °C using a Ti-70 Beckman Coulter rotor. The supernatant was discarded, and the pellets were resuspended using 1 mL of the NMR nondetergent buffer (50 mM Tris-base pH 7.5, 50 mM KCl, 1 mM EDTA) and then transferred into 1.5 mL Eppendorf tubes. Samples were repelleted using a benchtop centrifuge at 17,000 rpm for 30 min at 4 °C. Freeze−thaw cycles were performed three to four times for each sample to remove the excess buffer. The pellets were frozen and kept at −80 °C until needed. Samples were packed into a 1.6 mm rotor for direct polarization (DP) and temperature series experiments, with an estimated mass of 2.25 mg of protein, 2.25 mg of lipids, and ∼4.5 μL of buffer in each sample. A 3.2 mm rotor was used for U-^{13}C,^{15}N SM-KirBac1.1 and NA POPC/POPC:POPG in TEDOR experiments, with an estimated mass of 6 mg of protein, 6 mg of lipids, and ∼12 μL of buffer in each sample.

K^+ Efflux Assay. Assays were performed as previously described.[16,31,41,42] In summary, proteoliposomes were incubated with 100 μM 9-amino-6-chloro-2-methoxyacridine (ACMA) for 10−15 min and then were diluted with Na^+ buffer (20 mM Na-HEPES, 150 mM NaCl, 1 mM EDTA, pH 7.4) in a glass 96-well plate and again in a 384-well assay plate. Baseline fluorescence was acquired for 1 min followed by addition of 80 μM carbonyl-cyanide *m*-chlorophenylhydrazone (CCCP) to initiate flux. The fluorescence was read for 15 min, and then 10 nM valinomycin was added to each well to measure the maximum K^+ flux. All the data were normalized using the following equation:

$$F_N = (F - F_V)/(F_B - F_I) \quad (1)$$

where F_N stands for normalized fluorescence, F is the measured fluorescence of the sample, F_I is minimum fluorescence after adding the valinomycin, and F_B is the average of the baseline taken before adding the CCCP. Flux assay rates were fit to the following monoexponential decay function:

$$F_N = a^* \exp^{-t^*R} + c \quad (2)$$

where F_N is for normalized fluorescence, a is the preexponential factor, t is read time in seconds, R is the decay rate of fluorescent signal in seconds, and c is a constant.

SSNMR Spectral Acquisition. All MAS experiments were acquired on a 600 MHz Agilent DD2 spectrometer (Agilent Technologies, Santa Clara, CA, and Loveland, CO). The ^{13}C chemical shift was indirectly referenced to DSS using the downfield adamantane peak at 40.48 ppm.[43] All samples for 1D temperature series spectra and 2D DARR spectra were packed into 1.6 mm PENCIL rotors and were acquired with 12,000 Hz MAS rates in a 1.6 mm FAST-MAS probe. For FAST-MAS experiments, the ^{13}C 90° pulse width was set to 1.4 μs, and the ^{1}H 90° pulse width was set to 1.2 μs. The chemical shift of the water line with and without presaturation rf field strength at a duration equivalent to the ^{1}H decoupling field in all FAST-MAS experiments was acquired at pertinent set temperatures using a ^{1}H spin lock set at the aggregate decoupling B_1 field strength and duration.[44] All 1D DP experiments were acquired with 2048 scans and 21.6 kHz of SPINAL-64 decoupling[45] on ^{1}H. In DARR experiments, CP contact time was 2 ms. Tangent-ramped CP spin-lock power was set to 122.1 kHz for ^{1}H and 100.3 kHz for ^{13}C. Decoupling field strength was identical with 1D experiments. All 2D DARR spectra for PG assignments were acquired with 400 indirect dimension complex points, an indirect sweep width of 26,667 Hz, and 500 ms of DARR mixing time at a sample temperature of ∼10 °C, discussed below.

Z-filtered transferred echo double resonance (ZF-TEDOR)[46] ^{15}N-^{13}C spectra were acquired on uniformly U-^{13}C,^{15}N-labeled KirBac1.1 in the presence (3:2 PC/PG) and absence (PC only) of activating lipids. TEDOR spectrum samples were packed into a 3.2 mm PENCIL rotor and were acquired with 13,333 Hz magic-angle spinning (MAS) at a sample temperature ∼10 °C estimated based on our previously published temperature calibration profile for the probe in question.[47] For 3.2 mm BALUN TEDOR experiments, the ^{13}C 90° pulse width was set to 3.0 μs, the ^{1}H 90° pulse width was set to 2.3 μs, and the ^{15}N 90° pulse width was set to 5.4 μs. SPINAL-64 decoupling was set to 34.3 kHz. Spectra were acquired with a sweep width of 24,000 Hz and 96 complex points in the indirect dimension.

NCACX, NCOCX, and CaNcoCa experiments were described previously.[31] Briefly, samples were packed into a 3.2 mm PENCIL rotor, and data were collected at an expected sample temperature of ∼4 °C. These data sets were acquired using a BALUN HCN probe (Agilent Technologies, Loveland, CO). Each data set was acquired using nonuniform sampling (NUS) in both indirect dimensions with an overall coverage of 25%. For the NCACX experiment, the magic angle spinning (MAS) rate was set to 13,333 Hz. The NCOCX experiment used a MAS rate of 12,000 Hz. The CaNcoCA experiment used a MAS rate of 11,111 Hz.

NMR Data Analysis. The 1.6 mm FAST-MAS H_2O ^{1}H chemical shift with and without decoupling was used to calculate the sample temperature with and without decoupling according to the following equation:

$$\delta = 5.060 - 0.0122T + (2.11 \times 10^{-5})T^2 \quad (3)$$

where the difference between the two measurements represents the temperature contribution from RF heating.[44] The contribution to sample temperature from spinning rate was calculated based on the known profile of a 1.6 mm SSNMR probe according to the following equation:

$$T_{sample} = 0.98T_{set} + 3.79°C \times e^{\omega_r/19.6kHz} - 3.49°C \quad (4)$$

https://doi.org/10.1021/jacs.3c09266
J. Am. Chem. Soc. 2024, 146, 4421−4432

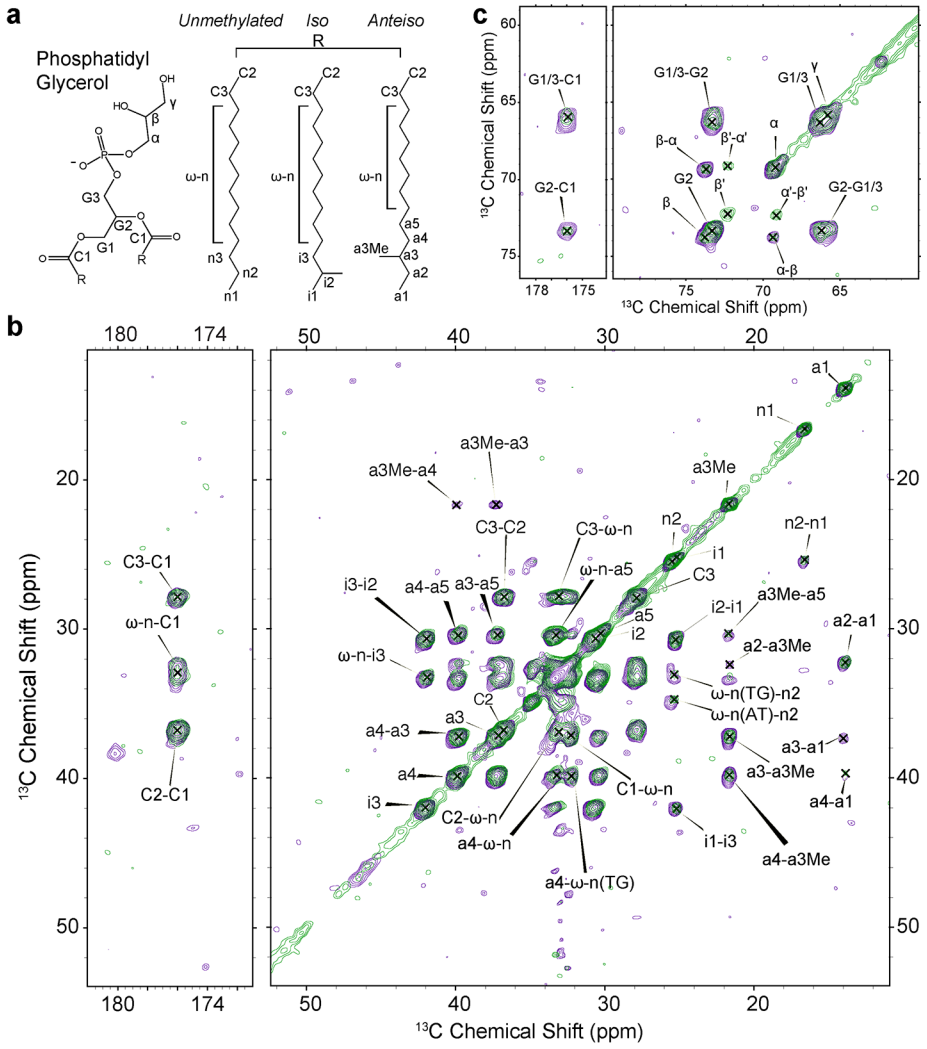

Figure 1. Chemical shift assignment of ^{13}C-PG lipids in the presence (green) and absence (purple) of NA-KirBac1.1. (a) Chemical structure of the PG lipids with three different isomers: unmethylated, iso (methylated at ω-1), and anteiso (methylated at ω-2), which were previously identified via gas chromatography.[25] (b) Acyl chain chemical shift assignments of the labeled PG in the presence (green) and absence (purple) of NA-KirBac1.1. (c) Chemical shift assignment of the glycerol headgroup of the labeled PG with and without NA-KirBac1.1. Samples are reconstituted with a 9:1 w/w ratio (10% X_{PG}) of POPC/PG for both samples, and the protein-containing sample was reconstituted at a protein/lipid ratio of 1:1 w/w, corresponding to a molar ratio of approximately 1:50.

where ω_r is the spinning rate in kHz.[48] 2D spectra were analyzed using NMRFAM-SPARKY.[49,50] 1D DP experiments were fit in NMRPipe[51] using the nonlinear spectral fitting package with error calculated as follows:

$$\text{Normalized error}_i = \text{noise}_i \times \frac{\left(\frac{\text{fitting error}}{\text{fit peak height}}\right)_i}{\text{fit peak intensity}_i} \quad (5)$$

where "fitting error/fit peak height" is the ratio of the nonlinear spectral modeling package fitting error calculated at each temperature "i" used to modify the estimated spectral noise "noise$_i$", normalized to the peak intensity.

Molecular Dynamics Simulation Analysis. The inactive-state structure of KirBac1.1 7SWJ[52] was aligned in the membrane using the PPM 2.0 Web server[53] prior to system production using Martini Maker[54,55] in CHARMM-GUI.[56,57] Systems were designed using a box size of 150 nm and 50 mM NaCl for production at 273.15 K. The bilayer environment consisted of POPC with varying concentrations of POPG. Minimization, equilibration, and production MD was performed in GROMACS version 2020 using the Martini2.2 force field.[58−60] Minimization and equilibration were performed with the Berendensen barostat,[61] v-rescale thermostat, and reaction-field electrostatics. Production MD used the same method except with the Berendensen thermostat. PyLipID[62] was used to calculate the residency time for PG per KirBac1.1 residue with interaction start and end cutoffs of 0.55 and 1.0 nm, respectively. Residency times for residues of interest were summed and fit to the Hill equation as a function of PG concentration, as described above.

RESULTS

Chemical Shift Assignments of Labeled PG. U-^{13}C-PG lipids were purified from *Staphylococcus simulans* as described previously.[25] We reconstituted these lipids into liposomes with and without NA-KirBac1.1 with a 9:1 ratio of 1-palmitoyl-2-oleoylphosphatidylcholine (POPC)/PG (10% X_{PG}). 2D ^{13}C−^{13}C DARR[63] experiments were performed on both samples. These spectra were acquired at a sample temperature of ∼−5 °C with 500 ms of mixing to capture most of the ^{13}C−^{13}C correlations (Figure 1, Figure S1). We assigned these U-^{13}C-PG lipid spin systems in the presence (green) and absence (purple) of NA wild-type KirBac1.1 containing the

https://doi.org/10.1021/jacs.3c09266
J. Am. Chem. Soc. 2024, 146, 4421−4432

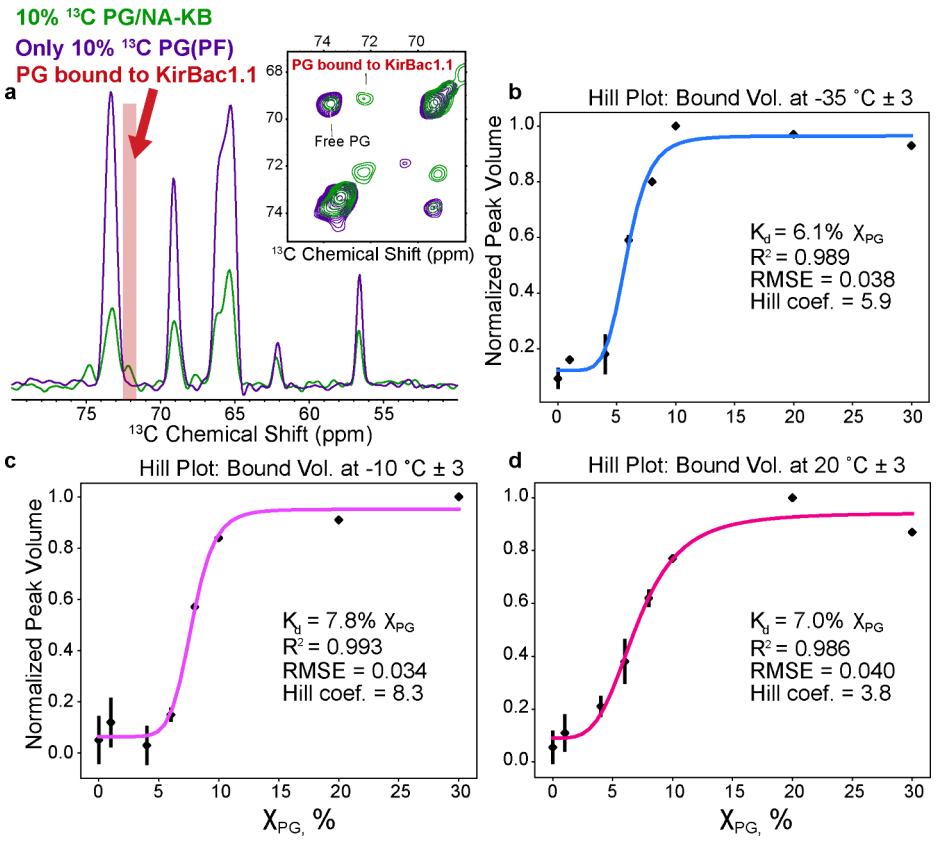

Figure 2. Affinity and cooperativity between KirBac1.1 and PG lipids. (a) 1D DP and 2D DARR spectra of 10% ^{13}C PG in the bilayer in the presence (green) and absence (purple) of NA-Kirbac1.1. The bound PG population can be found at ∼72 ppm, highlighted in red. (b, d) Calculated K_d and plots from Hill equation fits at different SSNMR sample temperatures. Error bars indicate normalized spectral noise-modified fitting error as described in Materials and Methods. Samples for 1D spectra were reconstituted at a lipid/protein ratio of 1:1 w/w corresponding to a molar ratio of approximately 50:1.

stability mutation I131C (WT-SM).[39] Chemical shift assignments are summarized in Table S1. Three acyl chain isomers were previously identified by van Beekveld et al. in PG lipids isolated from *S. simulans*, which were used in the present work: unmethylated (∼5%), anteiso (∼80%), and iso acyl chains (∼15%).[25] Of these, unmethylated lipids were found as C16:0 or C18:0, anteiso acyl chains were identified as C15:0 and C17:0, whereas iso acyl chains were observed to be C14:0, C15:0, C16:0, and C:17:0. Figure 1a shows the structure of the phosphatidylglycerol (PG) headgroup and glycerol backbone with these different isomers labeled. Figure 1b shows the full chemical shift assignments of the acyl tails and backbone carbonyls of the ^{13}C PG in the presence (green) and absence (purple) of NA-KirBac1.1. As before, we observe correlations indicating the presence of ordered, all-trans (AT) and more disordered, trans-gauche (TG) acyl chains.[16,41] We previously observed bilayer ordering as a byproduct of KirBac1.1-PG interaction, where the mutation of PG-interacting arginine residues significantly reduced the ordering effect.[16] Figure 1c shows the chemical shift assignments of the glycerol backbone and headgroup region of the ^{13}C-labeled PG. By overlaying the two spectra, we were able to identify the PG bound to KirBac1.1 population at ∼72 ppm that is absent in the KirBac1.1 free sample (PF, purple), denoted as PGβ'. We also observe a slight chemical shift perturbation (CSP) corresponding to the bound headgroup carbon α, designated as α'. As a final quality control step, purified PG lipids were assayed against synthetic lipids and were found to activate KirBac1.1 to a similar extent (Figure S2).

Determination of Binding Affinity. Completed chemical shift assignments found that the KirBac1.1-bound PG peak was cleanly resolved in one-dimensional (1D) spectra. Thus, 1D direct polarization (DP) experiments were acquired for proteoliposome samples containing increasing amounts of ^{13}C-PG (1, 4, 6, 8, 10, 20, and 30% X_{PG}) at sample temperatures of −35, −10, and 20 °C (Figure S3). Because the efficacy of cross-polarization (CP) is strongly entwined with dynamics, we hypothesized that the strength of the bound headgroup peak relative to unbound in DARR spectra could be overestimated because of the increased CP efficiency rather than be reflective of the actual bound peak volume. To counteract this inherent bias, we acquired the 1D series using DP rather than CP, which should not be biased by dynamics. Figure 2a depicts a representative zoomed-in view of the DP spectra of 10% X_{PG} ^{13}C-PG in the presence (green) and absence (purple) of KirBac1.1, and the marked area (red shade) represents the PG bound to the KirBac1.1 population at ∼72 ppm identified from 2D DARR experiments. We assumed that the nature of these interactions would be a function of both lipid−protein affinity and the rate of lipid diffusion, which would be reduced at a lower temperature. To investigate the fraction of bound population as a function of both ^{13}C-PG concentration and temperature, in each spectrum, the bound peak volume was fit using the nonlinear spectral fitting package in NMRPipe,[51] and the results were intriguing:

https://doi.org/10.1021/jacs.3c09266
J. Am. Chem. Soc. 2024, 146, 4421−4432

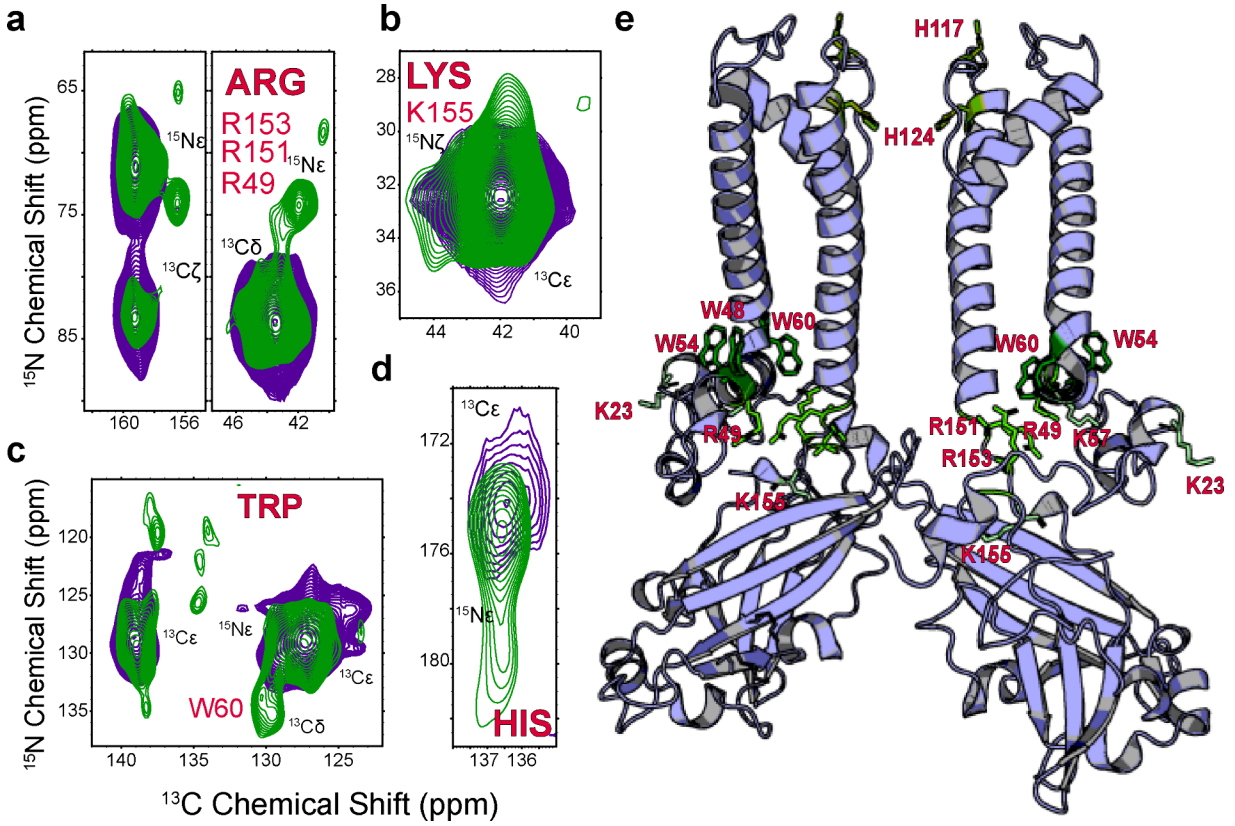

Figure 3. 2D TEDOR spectra of ^{13}C−^{15}N labeled KirBac1.1 reconstituted in the NA-POPC (purple) and NA-POPC/POPG (green) lipid bilayer. (a) Arginine residues 49, 151, and 153 in the identified cationic PG binding pocket. (b) Lysine 155 within the cationic pocket. (c) Tryptophan 54 and 60 in the slide helix. (d) Histidine ^{15}Nε outliers likely located on the extracellular face of the channel. (e) All residues are displayed on the full-length structural model of KirBac1.1 (7SWJ).[52] Samples were reconstituted in POPC only (purple) or 3:2 w/w ratio of POPC/POPG (green) and a lipid/protein ratio of 1:1 w/w corresponding to a molar ratio of approximately 50:1.

rather than a hyperbolic curve as expected, the results were sigmoidal, indicating positivity cooperativity. The Hill−Langmuir equation (eq 1) defines ligand occupancy (θ) as a function of the affinity (defined as the dissociation constant, K_d) and cooperativity (Hill coefficient, n) between two molecules as a function of ligand concentration:[4,5,64]

$$\theta = \frac{[L]^n}{[L]^n + K_d} \quad (6)$$

All bound ^{13}C-PG peak integrated intensities were normalized to the saturated occupancy and fit into the Hill−Langmuir equation to determine the K_d at all three sample temperatures (Figure 2b−d). We observed a sigmoidal curve in all cases with Hill coefficients from 3.8 to 8.3, indicating that PG association to the K^+ channel is positively cooperative. Binding of the first PG lipid to the channel will affect the structure of the second binding site, facilitating further binding and increasing affinity. This event will cause a series of changes and movement of the residues that are involved in gating and K^+ flux. Figure 3b−d shows the calculated K_d's from the Hill equation at sample temperatures of −35, −10, and 20 °C, which are 6.1, 7.8, and 7.0% X_{PG} in the bilayer, respectively. The K_d was stable relative to experimental error as a function of temperature; however, the cooperativity increased at the lower temperature within the liquid crystalline phase (−10 vs 20 °C) but then decreased again slightly in the gel phase (−35 °C). We interpret this to mean that effective lipid−protein stoichiometry will increase to a point when the kinetic energy associated with lipid phase is reduced.

Amino Acid Residue Side Chains Coordinate PG Lipids. As we previously established, arginine side chains are essential to gate KirBac1.1 in an activating lipid environment (POPC/POPG). We previously proposed that a cationic pocket in KirBac1.1 formed by R49, R151, and R153 moors the anionic lipid headgroups, which was confirmed via ^{13}C−^{31}P rotational echo double resonance (REDOR)[65] dephasing experiments between arginine Cζ and bound anionic phospholipid headgroups.[16] When these residues are mutated to glutamine, the channel is closed and inactive. Based on the mutational analysis in CGMD simulations, we also suggested that residues proximal to this arginine pocket may also play a role, either during the first steps of allosteric communication or as secondary residues supporting the pocket itself.[36] However, experimentally, we did not have a complete picture of lipid−protein interactions in the open-activated state of the channel. To better identify the full set of amino acid side chain interaction with lipid headgroups, we acquired 2D z-filtered transferred echo double resonance (zf-TEDOR) ^{15}N−^{13}C correlation spectra.[46] We reconstituted U-^{15}N,^{13}C-KirBac1.1 into either completely zwitterionic NA-POPC (purple) or 3:2 NA-POPC/POPG (green) proteoliposomes to identify the residues that recruit, coordinate, or tether PG lipids (Figure 3). CSPs between the TEDOR spectra of each sample cleanly identified residues that associate with anionic lipids and facilitate allosteric activation of the channel (Figures S4 and

https://doi.org/10.1021/jacs.3c09266
J. Am. Chem. Soc. 2024, 146, 4421−4432

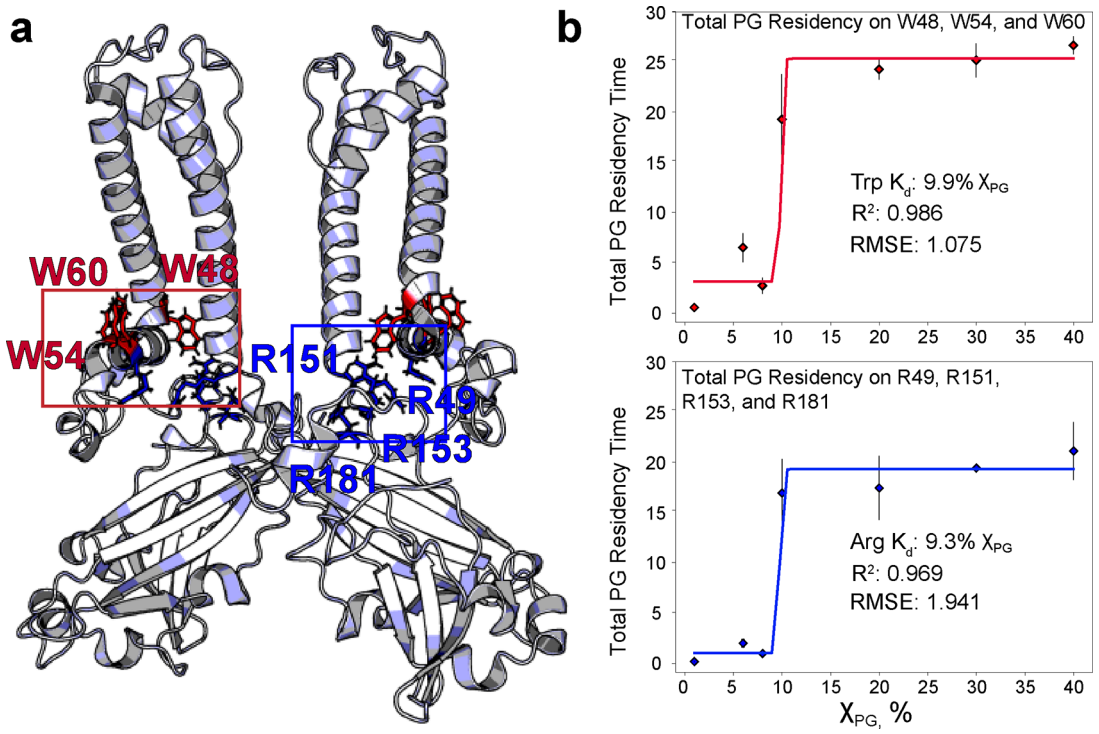

Figure 4. (a) KirBac1.1 structure (7SWJ) with highlighted residues. W48, W54, and W60 (red) and R49, R151, R153, and R181 (blue). (b) Total POPG residency time on tryptophan (top, red) and arginine residues (bottom, blue) as a function of the POPG concentration. When total residency times are fit to the Hill equation, a sigmoidal curve is observed with a calculated K_d of approximately 10% X_{PG}. Data in panel b are presented as mean ± s.d. from five independent replicates per PG concentration.

S5). Figure 3a depicts arginine $^{15}N\varepsilon$ outliers near ∼74 ppm that are present in a synthetic POPC/POPG lipid mixture but absent in the POPC mixture. Figure 3b,c presents the $^{13}C\varepsilon$ lysine and $^{13}C\delta$ tryptophan chemical shift outliers at ∼42 and 130 ppm, respectively. In Figure 3d, chemical shift perturbations in histidine side chains are observed.

Previously, we identified the arginine outliers in Figure 3a as R49, R151, and R153 via mutagenesis. Mutation of these residues to Gln abolished outlier signal in $^{15}N-^{13}C$ correlation spectra, which coincided with the complete loss of channel function.[16] Based on our previously published chemical shift assignments of the gating bundle and transmembrane region,[31] we assigned the outliers in Figure 3b,c as W60 and K155, which were confirmed via backbone and side chain resonance assignments in 3D spectra (Figures S6−S8). Chemical shift assignments are summarized in Tables S2 and S3. It was not immediately clear which His residue(s) was responsible for the CSPs observed in Figure 3d. Although the observed CSPs could be related to the 6x C-terminal His tag, that does not automatically rule out histidine residues involved in lipid regulation. The structure of KirBac1.1 is presented with these residues labeled in Figure 3e, as well as histidine residues that could give rise to CSPs in Figure 3d. Because K155 is within the cationic pocket formed by R49/151/153, we hypothesize that it is also involved in lipid gating. We previously observed that W60 had the tendency to move toward W48 of the adjacent subunit in CGMD, which was accompanied by some slide helix "sliding" motion. The extent of this motion was correlated to both PG residency time on gating arginines *in silico* and to total K^+ flux *in vitro*.[36] Here, we hypothesize that the mechanism of cooperativity, whereby lipid binding is communicated from subunit to subunit, is mediated through slide helix motion that functions to increase the accessibility of adjacent subunits' PG binding sites. It should be noted that the acyl tails for PG lipids in TEDOR samples differ from those presented in Figures 1 and 2. However, because purified lipids and synthetic POPG lipids activate KirBac1.1 to a similar extent (Figure S2), the observed CSPs are attributed to lipid binding and channel activation despite the small potential secondary effects the differences may have on biophysical properties of the system.

Coarse Grain Molecular Dynamics Predict Sigmoidal Lipid Residency. CG molecular dynamics (CGMD) simulations were performed in tandem to complement the NMR data analysis. We previously observed in MD calculations that residues involved in the allosteric network could be mutated to impact PG residency time and residue−residue contacts throughout the channel.[36] Thus, we hypothesized that we might observe interesting phenomena in CGMD PG titrations as well. Figure 4a shows the 7SWJ structure of KirBac1.1[52] with residues highlighted in red (tryptophan) and blue (arginine). This structure was inserted into CGMD systems consisting of POPC supplemented with increasing concentrations of POPG. Production MD was performed for 10 μs for five replicates using the Martini2.2 force field[58−60] in GROMACS.[66] POPG residency time throughout each replicate simulation for each residue was calculated using PyLipID[62] (Figure S9). Figure 4b presents the total PG residency time on W48, W54, and W60 (red) and R49, R151, R153, and R181 (blue) as a function of PG concentration. As with the experiments described above, we observed a sigmoidal curve but with a slightly larger K_d of approximately 10% X_{PG} for both arginine and tryptophan residues, in surprisingly good agreement with experimental results considering that this simulation time is not long enough to capture all the motions associated with channel gating.

https://doi.org/10.1021/jacs.3c09266
J. Am. Chem. Soc. 2024, 146, 4421−4432

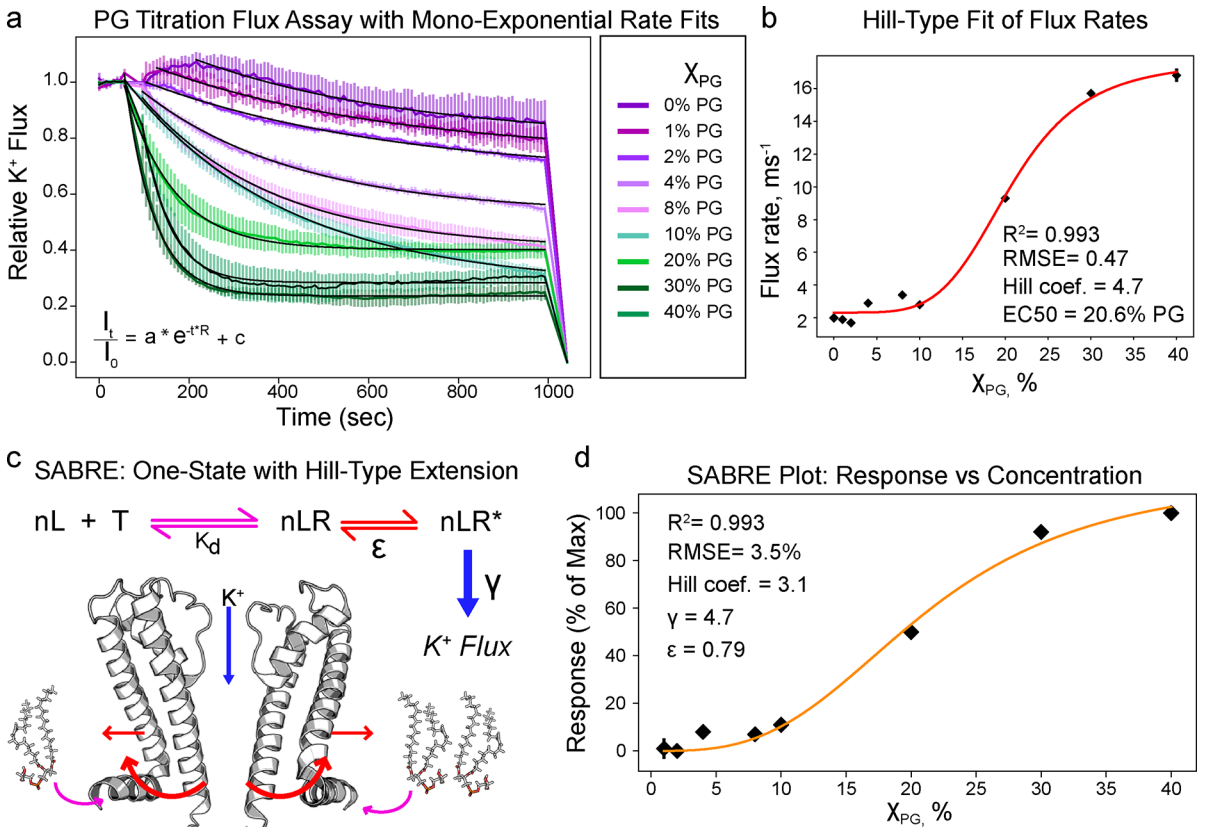

Figure 5. PG titration fluorescence K^+ flux assay of KirBac1.1 with monoexponential rate fits. (a) Normalized K^+ flux assay data as a function of the concentration of POPG. Data are presented as average ± s.d. across three replicates. Black lines indicate the monoexponential rate of flux, fit according to the inset equation. Samples were reconstituted in successively higher bilayer concentrations of POPG at a 200:3 lipid/protein ratio corresponding to a molar ratio of approximately 1000:3. (b) Hill equation fits of flux rates as a function of bilayer PG concentration, indicating an EC_{50} of 20.6% X_{PG}. Scatter points indicate the fit rate from ± RMSE in rate fitting from panel a. (c) Schematic illustrating the components of the SABRE equation. (d) SABRE plot correlating PG concentration to response. Scatter points indicate the fit rate from ±RMSE in rate fitting from panel a.

During previous CGMD analysis, as a function of mutations to the allosteric network, we concluded that activation *in silico* on this time scale was *not* observable. This observation could be related to slight differences in how PG interacts with the closed channel versus open channel. Alterations to physical membrane properties such as curvature (or lack thereof *in silico*), differences in acyl chain composition, and hydration levels between techniques could also play a role. Regardless, good agreement is observed between simulation and experimental results, which is encouraging. Analysis of possible PG-interacting His and Lys residues in the CGMD simulations of the closed state of KirBac1.1 did not find any significant lipid residency, indicating that CSPs observed in Figure 3c,d could result from lipid−protein interactions that occur downstream in the PG-driven activation pathway.

The Rate of K^+ Flux Has a Sigmoidal Response to PG Concentration. We performed fluorescence quenching K^+ flux assays to determine the effect of PG concentration on the activity of KirBac1.1 to understand the relationship between channel activity and cooperative lipid loading. A titration of POPG into POPC was performed over the same range of PG concentration as was used in NMR experiments. As expected, activity increased as PG concentration increased. Figure 5a illustrates this trend as PG concentration is elevated from 0 to 40 X_{PG}. In this figure, purple shades correspond to less activity and green shades correspond to more activity in the presence of PG. For each PG concentration, the rate of flux was then fit to a monoexponential decay equation (black lines over purple/green flux data). The resultant plot of flux rates as a function of PG concentration was, again, sigmoidal. We fit these rates to the Hill equation to determine the EC_{50} and cooperativity. In this regime, K_d is replaced with EC_{50}, the concentration of ligand that elicits 50% of the maximal cellular response:[67]

$$E/E_{max} = \frac{[L]^n}{[L]^n + EC_{50}^n} \quad (7)$$

The Hill coefficient/cooperativity fit to 4.7, which is close to the cooperativity observed from ssNMR data. However, the measured EC_{50} is 20.6 ± 0.5% X_{PG} (fit EC_{50} ± RMSE). Notably, this EC_{50} is within the physiological PG concentration that KirBac1.1 natively experiences in *Burkholderia pseudomalei* membranes.[68] A physiological EC_{50} within this range means that small changes in anionic lipid composition could lead to large changes in relative K^+ flux, indicative of a natural control mechanism to tightly regulate channel function with small changes in physiological PG concentration.

One will note that the EC_{50} at 20% X_{PG} and K_d at 7−8% X_{PG} are far from identical. This result is, however, not unexpected, as lipid loading and K^+ flux are two related but distinct phenomena. It should be noted that, at physiological temperatures, the EC_{50} from Figure 5b corresponds to the PG saturation point observed in Figure 2d. Likewise, PG K_d corresponds to the cusp of the observed activity thresholding

https://doi.org/10.1021/jacs.3c09266
J. Am. Chem. Soc. 2024, 146, 4421−4432

effect. Thus, channel activity accelerates only as the channel trends toward saturation in PG lipids. As above, we do note that the lipid/protein ratio necessary to resolve differences throughout the course of the flux assay (200:3 w/w) is quite different compared to NMR samples, and the POPG acyl tails differ from those presented in Figures 1 and 2. Because both synthetic and purified lipids similarly activate the channel, the observed results are expected to be mediated primarily through lipid binding, but additional contributions from alterations to membrane properties can and should not be ruled out.

To investigate their relationship, we implement the receptor theory that, generally, describes the relationship between ligand−receptor K_d and postsignal transduction cellular response.[69] This treatment has also been successfully applied to ligand-gated ion channels[70,71] and can be modified to incorporate Hill-type cooperativity. Here, we implement the SABRE (Signal Amplification (γ), Binding affinity (K_d), and Receptor activation Efficacy (ε); Figure 5c) methodology, pioneered by Peter Buchwald,[38] to investigate:

$$E/E_{max} = \frac{\varepsilon\gamma[L]^n}{(\varepsilon\gamma - \varepsilon + 1)[L]^n + K_d^n} \quad (8)$$

In this equation, each individual parameter is tied to an individual step: K_d for ligand-binding affinity, ligand efficacy (ε) for channel activation, and amplification (γ) for channel flux. The Hill coefficient n is introduced to fit sigmoidal results that describe a nonlinear response to ligand concentration $[L]$. In this regime, ε ranges from 0, describing an antagonist, to 1, describing a full agonist. Values $0 < \varepsilon < 1$ describe partial agonism. γ describes the functional response of the channel to the ligand and ranges from 1 (linear response) to infinity (cooperative response). From fitting of the X_{PG} response curve (Figure 5c), we observe an ε value of 0.79, a γ value of 4.7, and a Hill coefficient of 3.1. A ligand efficacy of 0.8 indicates that PG is a strong but partial agonist; the amplification and Hill-type coefficient further establish strong cooperativity. It is interesting that all of the K^+ flux assays we performed both here and in our previous studies reveal a maximum of ∼80% of total possible flux in the presence of simple PG lipids, which could be related to PG as a strong but partial agonist. Our chemical shift assignments of the PG-bound state of KirBac1.1 revealed a minor and major conformation within the transmembrane region that stretched between the helical bundle crossing near the cationic lipid binding pocket and the selectivity filter.[31] Thus, our SABRE analysis could corroborate the existence of this PG lipid-associated but inactive state of KirBac1.1.

DISCUSSION

Allostery is a fundamental regulation mechanism that tightly controls key biological processes. Over the past several decades, it became clear that intersubunit and protein-stimulus cooperativity is fundamental to the regulation of K^+ flux through multiple classes of K^+ channels. The first functional reports of GIRK channels found that activated $G_{\beta\gamma}$ bound cooperatively,[7,8] K_v channel voltage sensors also activate cooperatively,[6] and targeted mutations and antibodies revealed that $K_{ir}2$ channels may be cooperatively and allosterically gated by PIP_2.[12] This classical allosteric picture in retrospect seems obvious as K^+ channels share a tetrameric structure characteristic of the original proteins for which this phenomenon was described.[4,5] However, what is novel in this study is that the observed cooperativity in lipid−protein interactions is tied directly to protein structure−function relationships, which then relates these discrete binding events directly to channel activity.

In past studies, either the K_d of a binding ligand or the EC_{50} corresponding to a gating stimulus was described. Here, we were able to unite these concepts and explicitly determine the degree of lipid-binding cooperativity in each case. In this process, we identified arginine, lysine, histidine, and tryptophan residues that either directly associate with PG lipids or undergo conformational perturbation as a consequence of lipid−protein interaction. These measurements confirmed previous SSNMR observations, CGMD simulations, and functional measurements of channel mutants. The cationic residues (Arg, Lys, and His) directly interact with anionic lipid headgroups in a similar manner to human Kir channel activation by PIP_2. Past work further suggests that these interactions are also correlated to the dewetting of these regions of the protein,[16] which would increase the strength of these Coulombic forces.

Another important observation is the role of interfacial tryptophan residues for anionic lipid recruitment and channel activation. This was partially predicted by two of our recent studies. In the first, we identified the cholesterol recognition motif in KirBac1.1, which included tryptophan residues at the lipid−water interface.[42] In the second, we used CGMD and observed that lipid residency times on these interfacial tryptophans were comparable to those observed for arginine residues known to be crucial to gating.[36] In most mammalian Kir channels, several conserved Trp residues, especially the site corresponding to W60 in KirBac1.1, are located at the ends of transmembrane α-helices. These tryptophan residues are hypothesized to act as floats, anchoring the helices into the membrane.[72] For example, in the archetypical K^+ channel KcsA, mutation of the tryptophan at this site decreases the open probability for the channel in POPG-rich bilayers.[72] A study in $K_{ir}6.2$ shows that this residue (W68) acts as a gatekeeper and mutation disrupts channel gating.[73]

Thus far, we have generally considered only the cooperative interaction between the PG headgroups and KirBac1.1 that leads to allosteric activation and K^+ flux. However, we have previously documented KirBac's ability to coordinate the physical properties of the membrane environment, which is driven by protein−lipid tethering.[16,41] Specifically, when PG-interacting arginine residues (Figure 3a) are mutated to glutamine, the loss of PG interaction coincides with an impaired ordering effect on the bilayer. Thus, it is hypothesized that coordination of physical membrane properties is at least in part a byproduct of anionic lipid binding. Although not explicitly interrogated here, the presence of AT acyl populations in the DARR spectra (Figure 1) does indicate that such an effect is observable. Necessary concessions in experimental conditions across techniques such as acyl chain composition, lipid/protein ratios, and potential hydration states may contribute to altered physical properties as well. Although the present work is invaluable in delineating cooperativity in lipid loading, the reader should be aware that these imitations do exist. Because the two are strongly entwined, the relationship between cooperative lipid loading and protein-driven bilayer ordering is an inherently complex topic, and deconvolution will therefore be an exciting avenue for future work.

https://doi.org/10.1021/jacs.3c09266
J. Am. Chem. Soc. 2024, 146, 4421−4432

CONCLUSIONS

Membrane proteins are functionally dependent upon their lipid environment, and interrogating the structure−function of proteins in their natural surroundings is essential. In this work, we used SSNMR, simulations, and functional measurements to understand how lipids regulate and direct K^+ flux through KirBac1.1. This is one of the first examples of direct lipid−protein cooperativity that is tied directly to functional activity. Based upon the established homology and functional similarity of KirBac1.1 to other channels in the K_{ir} family, this work suggests that tight regulation of membrane lipid composition is a key means by which organisms can regulate processes carried out by lipid-dependent membrane proteins. Indeed, the anionic lipid mole percentage corresponding to our measured EC_{50} is squarely within the physiological range of these lipids in *Burkholderia pseudomallei* and other Gram-negative bacteria. In humans, the PA, PG, and PIP_2 lipids on which TREK and Kir channels often depend are tightly regulated, which strongly suggest that the regulation of bilayer concentration is an essential means for an organism to control key physiological processes. The techniques and methodology presented above may be leveraged in the future to explicitly probe the structure−activity of these lipid−protein interactions.

ASSOCIATED CONTENT

Supporting Information

The Supporting Information is available free of charge at https://pubs.acs.org/doi/10.1021/jacs.3c09266.

Full 2D DARR, 2D TEDOR, and 1D DP spectra of ^{13}C-labeled lipids and KirBac1.1 at various concentrations, highlighting bound lipid peaks and corresponding chemical shift perturbations in protein spectra; chemical shift assignment tables and 3D strip plots depicting SSNMR resonance assignments of KirBac1.1 slide helix residues V47-V62 and lipid-binding pocket residues R148-I156; and full plots of PG residency time per residue derived from CGMD experiments (PDF)

AUTHOR INFORMATION

Corresponding Author

Benjamin J. Wylie − *Department of Chemistry and Biochemistry, Texas Tech University, Lubbock, Texas 79409, United States;* orcid.org/0000-0001-8183-2762; Email: Benjamin.J.Wylie@ttu.edu

Authors

Maryam Yekefallah − *Department of Chemistry and Biochemistry, Texas Tech University, Lubbock, Texas 79409, United States*

Evan J. van Aalst − *Department of Chemistry and Biochemistry, Texas Tech University, Lubbock, Texas 79409, United States*

Roy A. M. van Beekveld − *Department of Chemistry, Faculty of Science, Utrecht University, Utrecht 3584 CH, The Netherlands*

Isaac R. Eason − *Department of Chemistry and Biochemistry, Texas Tech University, Lubbock, Texas 79409, United States*

Eefjan Breukink − *Membrane Biochemistry and Biophysics, Department of Chemistry, Utrecht University, Utrecht 3584 CH, The Netherlands*

Markus Weingarth − *Department of Chemistry, Faculty of Science, Utrecht University, Utrecht 3584 CH, The Netherlands;* orcid.org/0000-0003-0831-8673

Complete contact information is available at: https://pubs.acs.org/10.1021/jacs.3c09266

Author Contributions

‖M.Y. and E.J.v.A. contributed equally to this work.

Funding

This work was funded by NIH grant R35GM124979 (Maximizing Investigators' Research Award [MIRA] R35) to B.J.W. This project has also received funding from the European Union's Horizon Europe grant and innovation program under grant agreement no. 101045485 to M.W.

Notes

The authors declare no competing financial interest.

ACKNOWLEDGMENTS

We thank Shane Scoggin and Naima Moustaid-Moussa for providing access to a plate reader for fluorescence assays. We would like to thank the Texas Tech High Performance Computing Center for providing computational time to run simulations and perform analysis.

REFERENCES

(1) Robinson, A. E.; Henderson, J. P.; Henzler-Wildman, K. A. A mass spectrometry based transport assay for studying EmrE transport of unlabeled substrates. *Anal. Biochem.* **2018**, *549*, 130−135.

(2) Rosenbaum, D. M.; Rasmussen, S. G.; Kobilka, B. K. The structure and function of G-protein-coupled receptors. *Nature* **2009**, *459* (7245), 356−63.

(3) Levental, I.; Lyman, E. Regulation of membrane protein structure and function by their lipid nano-environment. *Nat. Rev. Mol. Cell Biol.* **2023**, *24* (2), 107−122.

(4) Hill, A. V. The mode of action of nicotine and curari, determined by the form of the contraction curve and the method of temperature coefficients. *J. Physiol* **1909**, *39* (5), 361−73.

(5) Hill, A. V. The Combinations of Haemoglobin with Oxygen and with Carbon Monoxide. *I. Biochem J.* **1913**, *7* (5), 471−80.

(6) Tytgat, J.; Hess, P. Evidence for Cooperative Interactions in Potassium Channel Gating. *Nature* **1992**, *359* (6394), 420−423.

(7) Ito, H.; Sugimoto, T.; KobayashiI, I.; Takahashi, K.; Katada, T.; Ui, M.; Kurachi, Y. On the Mechanism of Basal and Agonist Induced Activation of the G-protein Gated Muscarinic K+ Channel in Atrial Myocytes of Guniea Pig heart. *J. Gen. Physiol.* **1991**, *98* (3), 517−533.

(8) KURACHI, Y.; ITO, H.; Sugimoto, T. Positive Cooperativity in Activation of the Cardiac Muscarinic K+ Channel by Intracellular GTP. *Pflugers Archiv-European Journal of Physiology* **1990**, *416* (1−2), 216−218.

(9) Qian, X.; Niu, X.; Magleby, K. Intra- and intersubunit cooperativity in activation of BK channels by Ca2+. *J. Gen. Physiol.* **2006**, *128* (4), 389−404.

(10) Niu, X.; Magleby, K. Stepwise contribution of each subunit to the cooperative activation of BK channels by Ca2+. *Proc. Natl. Acad. Sci. U.S.A.* **2002**, *99* (17), 11441−11446.

(11) D'Avanzo, N.; Cheng, W. W. L.; Doyle, D. A.; Nichols, C. G. Direct and Specific Activation of Human Inward Rectifier K+ Channels by Membrane Phosphatidylinositol 4,5-Bisphosphate. *J. Biol. Chem.* **2010**, *285* (48), 37129−37132.

(12) Xie, L.; John, S.; Ribalet, B.; Weiss, J. Phosphatidylinositol-4,5-bisphosphate (PIP(2)) regulation of strong inward rectifier Kir2.1 channels: multilevel positive cooperativity. *Journal of Physiology-London* **2008**, *586* (7), 1833−1848.

(13) Lopatin, A. N.; Makhina, E. N.; Nichols, C. G. Potassium channel block by cytoplasmic polyamines as the mechanism of intrinsic rectification. *Nature* **1994**, *372* (6504), 366−9.

(14) Hibino, H.; Inanobe, A.; Furutani, K.; Murakami, S.; Findlay, I.; Kurachi, Y. Inwardly rectifying potassium channels: their structure, function, and physiological roles. *Physiol Rev.* **2010**, *90* (1), 291−366.
(15) Roselle Abraham, M.; Jahangir, A.; Alekseev, A. E.; Terzic, A. Channelopathies of inwardly rectifying potassium channels. *Faseb J.* **1999**, *13* (14), 1901−1910.
(16) Borcik, C. G.; Versteeg, D. B.; Amani, R.; Yekefallah, M.; Khan, N. H.; Wylie, B. J. The Lipid Activation Mechanism of a Transmembrane Potassium Channel. *J. Am. Chem. Soc.* **2020**, *142* (33), 14102−14116.
(17) Hansen, S. B.; Tao, X.; MacKinnon, R. Structural basis of PIP2 activation of the classical inward rectifier K+ channel Kir2.2. *Nature* **2011**, *477* (7365), 495−U152.
(18) Whorton, M. R.; MacKinnon, R. Crystal structure of the mammalian GIRK2 K+ channel and gating regulation by G proteins, PIP2, and sodium. *Cell* **2011**, *147* (1), 199−208.
(19) Clarke, O.; Caputo, A.; Hill, A.; Vandenberg, J.; Smith, B.; Gulbis, J. Domain reorientation and rotation of an intracellular assembly regulate conduction in Kir potassium channels. *Cell* **2010**, *141* (6), 1018−1029.
(20) Huang, C.; Feng, S.; Hilgemann, D. Direct activation of inward rectifier potassium channels by PIP2 and its stabilization by G beta gamma. *Nature* **1998**, *391* (6669), 803−806.
(21) Soom, M.; Schonherr, R.; Kubo, Y.; Kirsch, C.; Klinger, R.; Heinemann, S. Multiple PIP2 binding sites in Kir-2.1 inwardly rectifying potassium channels. *Febs Letters* **2001**, *490* (1−2), 49−53.
(22) Meng, X. Y.; Zhang, H. X.; Logothetis, D. E.; Cui, M. The molecular mechanism by which PIP(2) opens the intracellular G-loop gate of a Kir3.1 channel. *Biophys. J.* **2012**, *102* (9), 2049−59.
(23) Jin, R.; He, S.; Black, K. A.; Clarke, O. B.; Wu, D.; Bolla, J. R.; Johnson, P.; Periasamy, A.; Wardak, A.; Czabotar, P.; Colman, P. M.; Robinson, C. V.; Laver, D.; Smith, B. J.; Gulbis, J. M. Ion currents through Kir potassium channels are gated by anionic lipids. *Nat. Commun.* **2022**, *13* (1), 490.
(24) Wang, W.; Touhara, K. K.; Weir, K.; Bean, B. P.; MacKinnon, R. Cooperative regulation by G proteins and Na+ of neuronal GIRK2 K+ channels. *Elife* **2016**, *5*, No. e15751.
(25) van Beekveld, R. A. M.; Derks, M. G. N.; Kumar, R.; Smid, L.; Maass, T.; Medeiros-Silva, J.; Breukink, E.; Weingarth, M. Specific Lipid Studies in Complex Membranes by Solid-State NMR Spectroscopy. *Chemistry* **2022**, *28* (70), No. e202202472.
(26) Kuo, A.; Gulbis, J. M.; Antcliff, J. F.; Rahman, T.; Lowe, E. D.; Zimmer, J.; Cuthbertson, J.; Ashcroft, F. M.; Ezaki, T.; Doyle, D. A. Crystal Structure of the Potassium Channel KirBac1.1 in the Closed State. *Science* **2003**, *300*, 1922−1926.
(27) Fürst, O.; Mondou, B.; D'Avanzo, N. Phosphoinositide regulation of inward rectifier potassium (Kir) channels. *Front. Physiol.* **2014**, *4*, 404.
(28) Borcik, C. G.; Eason, I. R.; Yekefallah, M.; Amani, R.; Han, R.; Vanderloop, B. H.; Wylie, B. J. A Cholesterol Dimer Stabilizes the Inactivated State of an Inward-rectifier Potassium Channel. *Angew. Chem., Int. Ed. Engl.* **2022**, *61* (13), No. e202112232.
(29) Singh, D. K.; Enkvetchakul, D.; Nichols, C. G.; Levitan, I. Kirbac 1.1 activity in liposomes is suppressed by cholesterol. *Biophys. J.* **2009**, *96* (3), 467a−467a.
(30) Singh, D. K.; Rosenhouse-Dantsker, A.; Nichols, C. G.; Enkvetchakul, D.; Levitan, I. Direct regulation of prokaryotic Kir channel by cholesterol. *J. Biol. Chem.* **2009**, *284* (44), 30727−36.
(31) Amani, R.; Borcik, C.; Khan, N.; Versteeg, D.; Yekefallah, M.; Do, H.; Coats, H.; Wylie, B. Conformational changes upon gating of KirBac1.1 into an open-activated state revealed by solid-state NMR and functional assays. *Proc. Natl. Acad. Sci. U. S. A.* **2020**, *117* (6), 2938−2947.
(32) Schmidpeter, P. A. M.; Petroff, J. T.; Khajoueinejad, L.; Wague, A.; Frankfater, C.; Cheng, W. W. L.; Nimigean, C. M.; Riegelhaupt, P. M. Membrane phospholipids control gating of the mechanosensitive potassium leak channel TREK1. *Nat. Commun.* **2023**, *14* (1), 1077.
(33) Cabanos, C.; Wang, M.; Han, X.; Hansen, S. B. A Soluble Fluorescent Binding Assay Reveals PIP2 Antagonism of TREK-1 Channels. *Cell Reports* **2017**, *20*, 1287−1294.
(34) Hansen, S. B. Lipid agonism: The PIP2 paradigm of ligand-gated ion channels. *Biochim. Biophys. Acta* **2015**, *1851* (5), 620−8.
(35) Cheng, W. W. L.; D'Avanzo, N.; Doyle, D. A.; Nichols, C. G. Dual-Mode Phospholipid Regulation of Human Inward Rectifying Potassium Channels. *Biophys. J.* **2011**, *100* (3), 620−628.
(36) Yekefallah, M.; Rasberry, C. A.; van Aalst, E. J.; Browning, H. P.; Amani, R.; Versteeg, D. B.; Wylie, B. J. Mutational Insight into Allosteric Regulation of Kir Channel Activity. *ACS Omega* **2022**, *7* (48), 43621−43634.
(37) Buchwald, P. Quantification of receptor binding from response data obtained at different receptor levels: a simple individual sigmoid fitting and a unified SABRE approach. *Sci. Rep* **2022**, *12* (1), 18833.
(38) Buchwald, P. A single unified model for fitting simple to complex receptor response data. *Sci. Rep* **2020**, *10* (1), 13386.
(39) Wang, S. Z.; Alimi, Y.; Tong, A.; Nichols, C. G.; Enkvetchakul, D. Stabilization of KirBac1.1 Tetramer by Blocking Ions. *Biophys. J.* **2009**, *96* (3), 467a−467a.
(40) Bligh, E. G.; Dyer, W. J. A Rapid Method of Total Lipid Extraction and Purification. *Can. J. Biochem. Physiol.* **1959**, *37* (8), 911−917.
(41) Borcik, C. G.; Versteeg, D. B.; Wylie, B. J. An Inward-Rectifier Potassium Channel Coordinates the Properties of Biologically Derived Membranes. *Biophys. J.* **2019**, *116* (9), 1701−1718.
(42) Borcik, C. G.; Eason, I. R.; Yekefallah, M.; Amani, R.; Han, R.; Vanderloop, B. H.; Wylie, B. J. A Cholesterol Dimer Stabilizes the Inactivated State of an Inward-rectifier Potassium Channel. *Angew. Chem., Int. Ed. Engl.* **2022**, *61* (13), No. e202112232.
(43) Morcombe, C.; Zilm, K. Chemical shift referencing in MAS solid state NMR. *J. Magn. Reson.* **2003**, *162* (2), 479−486.
(44) Gottlieb, H. E.; Kotlyar, V.; Nudelman, A. NMR Chemical Shifts of Common Laboratory Solvents as Trace Impurities. *J. Org. Chem.* **1997**, *62* (21), 7512−7515.
(45) Fung, B.; Khitrin, A.; Ermolaev, K. An improved broadband decoupling sequence for liquid crystals and solids. *J. Magn. Reson.* **2000**, *142* (1), 97−101.
(46) Jaroniec, C.; Filip, C.; Griffin, R. 3D TEDOR NMR experiments for the simultaneous measurement of multiple carbon-nitrogen distances in uniformly C-13, N-15-labeled solids. *J. Am. Chem. Soc.* **2002**, *124* (36), 10728−10742.
(47) van Aalst, E. J.; Borcik, C. G.; Wylie, B. J. Spectroscopic signatures of bilayer ordering in native biological membranes. *Biochim Biophys Acta Biomembr* **2022**, *1864* (6), No. 183891.
(48) Guan, X.; Stark, R. E. A general protocol for temperature calibration of MAS NMR probes at arbitrary spinning speeds. *Solid State Nucl. Magn. Reson.* **2010**, *38* (2−3), 74−6.
(49) Kneller, D.; Kuntz, I. UCSF SPARKY - An NMR display, annotation and assignment tool. *J. Cell. Biochem.* **1993**, 254−254.
(50) Lee, W.; Tonelli, M.; Markley, J. NMRFAM-SPARKY: enhanced software for biomolecular NMR spectroscopy. *Bioinformatics* **2015**, *31* (8), 1325−1327.
(51) Delaglio, F.; Grzesiek, S.; Vuister, G.; Zhu, G.; Pfeifer, J.; Bax, A. NMRPipe- A multidimensinoal spectral processing system based on Unix Pipes. *J. Biomol. Nmr* **1995**, *6* (3), 277−293.
(52) Amani, R.; Schwieters, C. D.; Borcik, C. G.; Eason, I. R.; Han, R.; Harding, B. D.; Wylie, B. J. Water Accessibility Refinement of the Extended Structure of KirBac1.1 in the Closed State. *Front Mol. Biosci* **2021**, *8*, No. 772855.
(53) Lomize, M. A.; Pogozheva, I. D.; Joo, H.; Mosberg, H. I.; Lomize, A. L. OPM database and PPM web server: resources for positioning of proteins in membranes. *Nucleic Acids Res.* **2012**, *40* (Database issue), D370−6.
(54) Qi, Y.; Ingolfsson, H. I.; Cheng, X.; Lee, J.; Marrink, S. J.; Im, W. CHARMM-GUI Martini Maker for Coarse-Grained Simulations with the Martini Force Field. *J. Chem. Theory Comput* **2015**, *11* (9), 4486−94.

https://doi.org/10.1021/jacs.3c09266
J. Am. Chem. Soc. 2024, 146, 4421−4432

(55) Hsu, P.; Bruininks, B. M. H.; Jefferies, D.; Cesar Telles de Souza, P.; Lee, J.; Patel, D. S.; Marrink, S. J.; Qi, Y.; Khalid, S.; Im, W. CHARMM-GUI Martini Maker for modeling and simulation of complex bacterial membranes with lipopolysaccharides. *J. Comput. Chem.* **2017**, *38* (27), 2354−2363.
(56) Lee, J.; Cheng, X.; Swails, J. M.; Yeom, M. S.; Eastman, P. K.; Lemkul, J. A.; Wei, S.; Buckner, J.; Jeong, J. C.; Qi, Y.; Jo, S.; Pande, V. S.; Case, D. A.; Brooks, C. L., 3rd; MacKerell, A. D., Jr.; Klauda, J. B.; Im, W. CHARMM-GUI Input Generator for NAMD, GROMACS, AMBER, OpenMM, and CHARMM/OpenMM Simulations Using the CHARMM36 Additive Force Field. *J. Chem. Theory Comput* **2016**, *12* (1), 405−13.
(57) Jo, S.; Kim, T.; Iyer, V. G.; Im, W. CHARMM-GUI: a web-based graphical user interface for CHARMM. *J. Comput. Chem.* **2008**, *29* (11), 1859−65.
(58) Monticelli, L.; Kandasamy, S. K.; Periole, X.; Larson, R. G.; Tieleman, D. P.; Marrink, S. J. The MARTINI Coarse-Grained Force Field: Extension to Proteins. *J. Chem. Theory Comput* **2008**, *4* (5), 819−34.
(59) Periole, X.; Cavalli, M.; Marrink, S. J.; Ceruso, M. A. Combining an Elastic Network With a Coarse-Grained Molecular Force Field: Structure, Dynamics, and Intermolecular Recognition. *J. Chem. Theory Comput* **2009**, *5* (9), 2531−43.
(60) de Jong, D. H.; Singh, G.; Bennett, W. F.; Arnarez, C.; Wassenaar, T. A.; Schafer, L. V.; Periole, X.; Tieleman, D. P.; Marrink, S. J. Improved Parameters for the Martini Coarse-Grained Protein Force Field. *J. Chem. Theory Comput* **2013**, *9* (1), 687−97.
(61) Berendsen, H. J.; Postma, J. V.; Van Gunsteren, W. F.; DiNola, A. R. H. J.; Haak, J. R. Molecular Dynamics with Coupling to an External Bath. *J. Chem. Phys.* **1984**, *81*, 3684−3690.
(62) Song, W.; Corey, R. A.; Ansell, T. B.; Cassidy, C. K.; Horrell, M. R.; Duncan, A. L.; Stansfeld, P. J.; Sansom, M. S. P. PyLipID: A Python Package for Analysis of Protein-Lipid Interactions from Molecular Dynamics Simulations. *J. Chem. Theory Comput* **2022**, *18* (2), 1188−1201.
(63) Takegoshi, K.; Nakamura, S.; Terao, T. C-13-H-1 dipolar-assisted rotational resonance in magic-angle spinning NMR. *Chem. Phys. Lett.* **2001**, *344* (5−6), 631−637.
(64) Langmuir, I. THE ADSORPTION OF GASES ON PLANE SURFACES OF GLASS, MICA AND PLATINUM. *J. Am. Chem. Soc.* **1918**, *40*, 1361−1403.
(65) Gullion, T.; Schaefer, J. Rotational-echo double-resonance NMR. *Journal of Magnetic Resonance (1969)* **1989**, *81* (1), 196−200.
(66) Abraham, M. J.; Murtola, T.; Schulz, R.; Páll, S.; Smith, J. C.; Hess, B.; Lindahl, E. GROMACS: High performance molecular simulations through multi-level parallelism from laptops to supercomputers. *SoftwareX* **2015**, *1−2*, 19−25.
(67) Buchwald, P. A three-parameter two-state model of receptor function that incorporates affinity, efficacy, and signal amplification. *Pharmacol. Res. Perspect* **2017**, *5* (3), No. e00311.
(68) Vanphung, L.; Chi, T.; Hotta, H.; Yabuuchi, E.; Yano, I. Cellular lipid and fatty acid compositions of *Burkholderia pseudomallei* strains isolated from a human and environment in Vietnam. *Microbiol. Immunol.* **1995**, *39* (2), 105−116.
(69) Buchwald, P. A Receptor Model With Binding Affinity, Activation Efficacy, and Signal Amplification Parameters for Complex Fractional Response Versus Occupancy Data. *Front. Pharmacol.* **2019**, *10*, 605.
(70) Kuwashima, Y.; Yanagawa, M.; Abe, M.; Hiroshima, M.; Ueda, M.; Arita, M.; Sako, Y. Comparative Analysis of Single-Molecule Dynamics of TRPV1 and TRPV4 Channels in Living Cells. *Int. J. Mol. Sci.* **2021**, *22* (16), 8473.
(71) Jarvis, G. E.; Thompson, A. J. Evidence for an effect of receptor density on ligand occupancy and agonist EC. *Sci. Rep* **2019**, *9* (1), 19111.
(72) Marius, P.; Zagnoni, M.; Sandison, M. E.; East, J. M.; Morgan, H.; Lee, A. G. Binding of anionic lipids to at least three nonannular sites on the potassium channel KcsA is required for channel opening. *Biophys. J.* **2008**, *94* (5), 1689−98.
(73) Männikkö, R.; Stansfeld, P. J.; Ashcroft, A. S.; Hattersley, A. T.; Sansom, M. S. P.; Ellard, S.; Ashcroft, F. M. A conserved tryptophan at the membrane-water interface acts as a gatekeeper for Kir6.2/SUR1 channels and causes neonatal diabetes when mutated. *J. Physiol.* **2011**, *589* (Pt 13), 3071−83.

https://doi.org/10.1021/jacs.3c09266
J. Am. Chem. Soc. 2024, 146, 4421−4432